Deformation Mechanism of Nylon 6/Layered Silicate Nanocomposites: Role of the Layered Silicate

G.-M. Kim, S. Goerlitz, G. H. Michler

Department of Physics, Martin Luther University at Halle–Wittenberg, D-06099 Halle (Saale), Germany

Received 23 March 2006; accepted 9 May 2006
DOI 10.1002/app.26067
Published online in Wiley InterScience (www.interscience.wiley.com).

ABSTRACT: Polymer/layered silicate nanocomposites, depending on the molecular weight of nylon 6 as the matrix, were prepared through melt blending with a twin-screw extruder to study their morphology and the role of layered silicates (i.e., montmorillonite) on local deformation processes. A thermal analysis of the nanocomposites was performed with differential scanning calorimetry. The dispersion of the layered silicates and nanocomposite morphology were investigated with wide-angle X-ray scattering and transmission electron microscopy. The results showed that the layered-silicate surfaces predominantly induced γ-form crystals of nylon 6, whereas α-form crystals were nucleated far away from the clay surface. The fraction of γ-form crystals and the degree of exfoliation increased with the molecular weight of the nylon 6 matrix. In a high-molecular-weight nanocomposite, a well-defined exfoliated nanomorphology was observed, in which fine nylon 6 lamellae were most likely to be oriented with their planes perpendicular to the injection-molding direction, although to a great extent the layered silicates were arranged on planes parallel to the injection-molding direction. On the contrary, a mixed nanomorphology appeared in a low-molecular-weight nanocomposite, intercalated and exfoliated nanomorphologies coexisting; the layered silicates were randomly dispersed in the nylon 6 matrix, and the nylon 6 lamellae grew in no preferential direction with respect to the layered-silicate surface. The dispersion of the layered silicates and the orientation of the layered silicates as well as the lamellae were directly reflected in the mechanical deformation processes. The results of *in situ* deformation experiments under a high-voltage electron microscope (1000 kV) indicated that the main deformation mechanism was microvoid formation either within the intercalated tactoids or in the vicinity of layered silicates in the matrix for intercalated and exfoliated nanomorphology systems, respectively. In the exfoliated nanocomposite, that is, the high-molecular-weight nanocomposite, the external applied stresses were much more effectively transferred from the polymer matrix to the layered silicates; furthermore, microvoid formation took place more uniformly and homogeneously throughout the deformed specimen, and thus a well-improved stiffness/ strength/ toughness balance was achieved in comparison with the mixed nanomorphology system (the low-molecular-weight nanocomposite). © 2007 Wiley Periodicals, Inc. J Appl Polym Sci 105: 38–48, 2007

Key words: morphology; nanocomposites; voids

INTRODUCTION

In recent years, hybrid organic–inorganic nanocomposites have attracted much attention because such hybrids may provide the possibility of controlled macroscopic physical properties through the tailoring of their morphologies at a molecular level. Conceptually, a polymer/layered silicate nanocomposite (PLSNC) is an assembly analogous to a fiber-reinforced polymer composite, but with an obvious difference in the length scale of the reinforcement. When we consider layered silicates (LSs) with a thickness of approximately 1 nm, a large aspect ratio (typically 100–1500), a high specific surface area (700–800 m^2/g), and geometrical percolation of the reinforcing elements may be considered reasonable assumptions to account for improved mechanical properties at very low contents, that is, a few weight percent.[1–9] One important result of the charged nature of LSs is that they generally possess highly hydrophilic features and therefore are naturally incompatible with a wide range of polymer types. A necessary prerequisite for the successful formation of PLSNCs is therefore the alteration of the polarity of LSs to make the LSs organophilic. Organophilic LSs can be produced from hydrophilic LSs by ion exchange with organic cations such as ω-amino acids [$H_3N^+(CH_2)_{n-1}COOH$], alkylammonium ions [$CH_3—(CH_2)_n—$], and silanes ($R—SiX_3$).[3,10–12] Synthetic approaches for PLSNCs have been well developed by several groups. In general, these methods achieve molecular-level incorporation of the LS [e.g., montmorillonite (MMT)] into the polymer by the addition of a modified silicate during the polymerization (*in situ* method),[13–16] to a solvent-swollen polymer,[6,17–20] or to

This article is dedicated to the memory of Dr. M. Kryszewski.

Correspondence to: G.-M. Kim (gyeong.kim@physik.uni-halle.de).

Journal of Applied Polymer Science, Vol. 105, 38–48 (2007)

TABLE I
Materials

Material	Supplier designation	Specification	Supplier
Low-molecular-weight nylon 6	Capron 8202	Number-average molecular weight = 16,400, meltflow index = 23.0	Honeywell
High-molecular-weight nylon 6	Capron B 135WP	Number-average molecular weight = 29,300, meltflow index = 1.2	Honeywell
$(HE)_2M_1R_1$	Bis(hydroxyethyl)(methyl)rapeseed quaternary ammonium organoclay	Organic loading = 95 mequiv/100 g of clay, organic content = 0 44.1 wt %	Southern Clay Products

a polymer melt.[21–28] The resulting PLSNCs can be classified into three general morphology classes. First, intercalated PLSNCs possess self-assembled, well-ordered, multilayered structures in which the extended polymer chains are inserted into the gallery between the LSs, but the LSs still have a well-defined spatial relationship with one another. Second, when the interaction between LSs exceeds the van der Waals gaps,[6] an exfoliated PLSNC will be achieved. In an exfoliated structure, the LSs are completely separated, and the individual layers are distributed throughout the polymer matrix, but they may not be as well ordered as those in an intercalated structure. Third, there is the conventional composite, in which the LSs are not individually dispersed but rather are aggregated in the polymer matrix; therefore, they act similarly to conventional fillers.

Until now, intensive research efforts have been devoted to the characterization of the mechanical properties of PLSNCs as a function of the degree of exfoliation and type of organo-LS.[7] Also, the phase structures of these materials have been intensively investigated with wide-angle X-ray scattering (WAXS), small-angle X-ray scattering,[29,30] transmission electron microscopy (TEM), Fourier transform infrared spectroscopy, and nuclear magnetic resonance.[31,32] However, the mechanisms responsible for the improvement of the mechanical properties have still not been identified. In general, the presence of inorganic filler particles influences directly the crystallization behavior of the polymer matrix. It is most likely that because the thickness of an LS is comparable to the gallery spacing between the LSs, which is even smaller than the radius of gyration of typical polymers, the phase morphology of PLSNCs may be more complex than that of conventional polymer composites. After the introduction of nano-LSs, the changes in the morphology of a polymer matrix may directly be reflected in a variety of deformation mechanisms, which lead in turn to remarkable differences in the ultimate mechanical properties of the materials.[33] To improve and control the ultimate mechanical properties for a wide range of applications and in particular to optimize the stiffness/toughness balance, a better understanding of the interrelationship between the morphology, mechanical deformation processes, and macroscopic properties is clearly required. Along these lines, in this work, we attempt first to study the morphology of nylon 6/clay nanocomposites, varying the molecular weight of the nylon 6 matrix, and then to study the exact role of LSs in the matrix as well as the effect of interfacial interactions between the LSs and polymer matrix during deformation processes. On the basis of these results, we can determine which factors may cause improvements in the properties of PLSNCs.

EXPERIMENTAL

Materials

The materials used in this study are described in Table I. Commercial grades of nylon 6 were chosen to span the range of melting viscosities commonly used in commercial injection-molding and extrusion applications. The organoclay, designated here as $(HE)_2M_1R_1$, was formed by a cation-exchange reaction between sodium montmorillonite (cation-exchange capacity = 95 mequiv/100 g of clay) and bis(hydroxyethyl)(methyl)rapeseed quaternary ammonium chloride and was obtained from Southern Clay Products (Gonzales, TX). The two resulting PLSNCs are designated as a low-molecular-weight nanocomposite (LMW-NC) and a high-molecular-weight nanocomposite (HMW-NC) on the basis of their respective low- and high-molecular-weight nylon 6 grades.

Melt processing

Melt-blended composites were prepared with a Haake corotating, intermeshing twin extruder (length = 305 mm, length/diameter = 10) (Karlsruher, Germany). The screws were a modular design with various degrees of mixing along the length of the screws. Compounding was carried out at a barrel temperature of 240°C, a screw speed of 280 rpm, and a feed rate of 980 g/h. Before each melt-process-

TABLE II
Mechanical Properties of the Nylon 6/LS Nanocomposites

Nylon6/$(HE)_2M_1R_1$		Modulus (GPa)	Yield strength (MPa)	Elongation at break (%)	Izod impact strength (J/m)
LMW-NC	0.0 wt % LS	2.82	69.2	232	36.0
	3.2 wt % LS	3.65	78.9	12	32.3
HMW-NC	0.0 wt % LS	2.75	69.7	302	43.9
	3.2 wt % LS	3.92	84.9	119	44.7

The data were taken from ref. 9.

ing step, all polyamide-containing materials were dried in a vacuum oven at 80°C for a minimum of 16 h. Extruded composite pellets were injection-molded into standard tensile (ASTM D 638, type I) and Izod specimens (ASTM D 256) with an Arburg Allround 305-210-700 injection-molding machine (Loburg, Germany). Selected mechanical properties for the PLSNCs are listed in Table II.

WAXS

WAXS was conducted with a Seifert XRD 3000 (Ahrensburg, Germany) with Cu Kα radiation ($\lambda = 1.54056$ Å). The tube source was operated at 40 kV and 30 mA. Scans were run in the low-angle region of $2\theta < 10^\circ$ for the study of the LS dispersion and in the high-angle region of $10^\circ < 2\theta < 35^\circ$ for the nanomorphology affected by LSs at a step size of 0.05° and with a 1-s dwell time.

Differential scanning calorimetry (DSC)

DSC measurements were conducted to measure the melting temperature and crystallization temperature of PLSNCs, which depended on the molecular weights of the matrix polymers, with a PerkinElmer DSC 7 (Waltham, MA) under a nitrogen atmosphere. The samples were sealed in aluminum pans and were heated and cooled in the DSC instrument at a rate of 10°C/min with sample masses of about 7 mg. The DSC temperature and heat flow values were calibrated with an indium standard. All experiments were carried out with the following procedures. The specimens were heated to 250°C at a rate of 10°C/min and held for 3 min to remove the residual crystals, which could be seeds for the following crystallization. The samples were then cooled to 15°C at a rate of 10°C/min.

TEM for morphology

The dispersion of the LSs and their distribution in the nylon 6 matrix were examined with TEM. To study how the LSs influenced the phase morphology of the nylon 6 matrix, the samples were chemically selectively stained with osmium tetroxide (OsO_4). For both studies, ultrathin sections ranging in thickness from 50 to 60 nm were cut with a Leica Ultracut E microtome (Wien, Austria). Sections were collected on 300-mesh copper TEM grids and examined by TEM with a JEOL 2010 transmission electron microscope (Tokyo, Japan) with an acceleration voltage of 200 kV.

High-voltage electron microscopy (HVEM) for mechanical deformation processes

To study mechanical deformation processes, samples were cryogenically microtomed at −100°C to thicknesses of about 400 nm. The thin sections were transformed on metal tape containing punched holes of 1 mm, deformed with a tensile device, and investigated *in situ* with HVEM at an acceleration voltage of 1000 kV. In comparison with conventional TEM, the higher acceleration voltage of HVEM led to lower inelastic scattering of the electrons. Consequently, the thickness of the specimens could be increased, and the irradiation damage could be reduced. All deformation tests under the microscope were performed at room temperature.

All the samples for WAXS, DSC, TEM, and HVEM were prepared from the same area at a depth one-third from the surface of an Izod bar to minimize the differences caused by the process conditions.

RESULTS

WAXS

To study the extent of the dispersion of LSs in PLSNCs with nylon 6 matrices of various molecular weights, first, WAXS measurements were carried out. From a general point of view, reflections in the low-angle region ($2\theta < 10^\circ$), indicating the confined *d*-spacing (basal spacing) between the silicate layers, are characteristic of the ordered, intercalated LSs in the matrix. On the contrary, the peaks for $2\theta > 10^\circ$ give information on the phase structure of the polymer matrix in PLSNCs. Figure 1 shows the X-ray diffraction traces in a low-angle region for an LMW-NC and an HMW-NC containing 3.2 wt % MMT. In the HMW-NC, WAXS does not produce well-defined

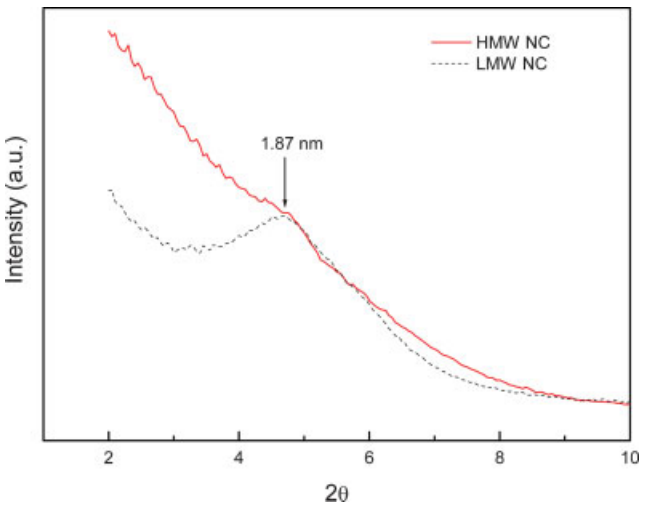

Figure 1 WAXS scans in low-angle regions for the LMW-NC and HMW-NC. [Color figure can be viewed in the online issue, which is available at www.interscience.wiley.com.]

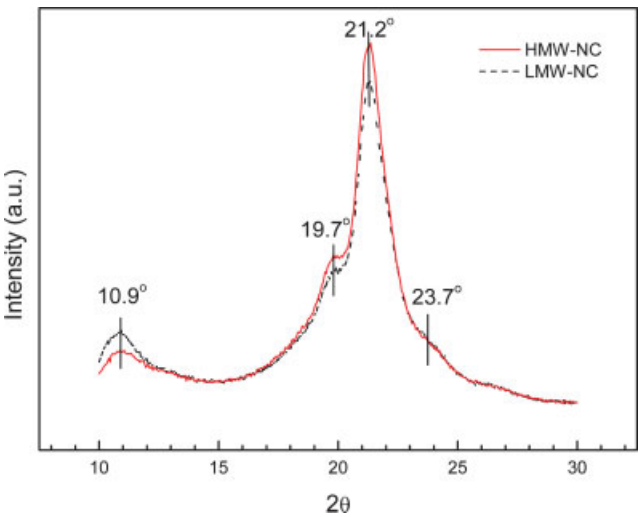

Figure 2 WAXS scans in high-angle regions for the LMW-NC and HMW-NC. [Color figure can be viewed in the online issue, which is available at www.interscience.wiley.com.]

basal reflections and, in fact, produces a featureless pattern for a typical exfoliated nanocomposite. This clearly indicates that the LSs are entirely exfoliated in the nylon 6 matrix. However, for the LMW-NC, the reflection peak appears at $2\theta = 4.7^\circ$, corresponding to a d_{001} basal spacing of 18.0 Å. Compared with the peak for the pristine organoclay from the previous study, [28] the organoclay pattern reveals a broad, intense peak around $2\theta = 5^\circ$, and the peak in the LMW-NC is shifted to a lower 2θ value, indicating that the interlayer spacing of LS stacks is slightly swollen from 18.0 to 18.7 Å. This result suggests that nylon 6 has penetrated the silicate interlayer spacing. At $2\theta < 5^\circ$, the intensity falls with a decreasing angle until approximately 3°, at which the intensity begins to rise again. This suggests that in the LMW-NC, there is a mixed nanomorphology, coexisting intercalated tactoids and exfoliated stacks of layers, as discussed later in the nanomorphology section.

It has been recently well established that the LSs drastically alter the morphology of nylon 6 even at low LS contents.[31,33,34] We have, therefore, explored the phase structure in nylon 6 matrices based on different molecular weights in the presence of LSs. Information on the phase structures stemming from the nylon matrix can readily be revealed in the high-angle region ($2\theta > 10$) in WAXS patterns, the results being shown in Figure 2. One substantial peak at $2\theta = 21.2^\circ$ and a relatively small peak at 10.9° are apparent; they have predominantly resulted from the γ-form crystal of nylon 6. Even with these peaks, small shoulders at $2\theta = 19.7^\circ$ and $2\theta = 23.7^\circ$ also appear in the X-ray diffraction traces. This pair of peaks is a distinctive feature of the {200} and {002} planes in the α-form crystals. On the basis of the WAXS results, we can conclude that although two crystal phases of nylon 6 coexist, the peak profiles clearly indicate that both PLSNCs predominantly contain the γ form.

DSC

To investigate the thermal behavior, such as the melting, crystallization, and formation of crystalline structures, we have performed DSC measurements. Figure 3 shows the DSC thermograms for both PLSNCs studied here. Over the DSC operating temperature range, the silicate layers do not exhibit any thermal transition. Thus, the events observed by

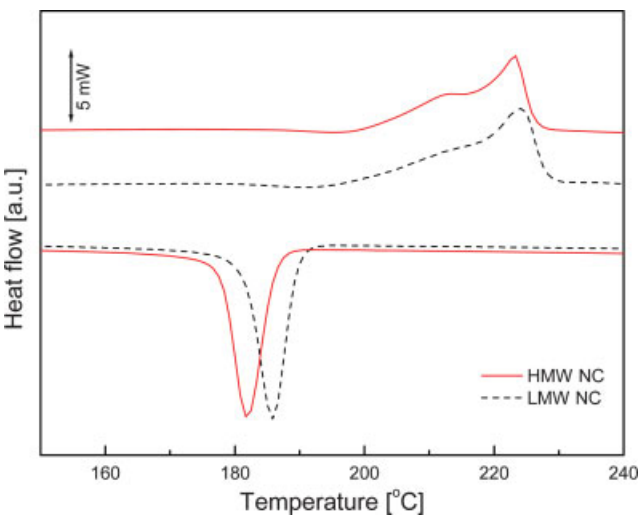

Figure 3 DSC thermograms for the LMW-NC and HMW-NC. [Color figure can be viewed in the online issue, which is available at www.interscience.wiley.com.]

DSC for PLSNCs are entirely related to the thermal behavior of the nylon 6 crystallites.

The most interesting feature from DSC is that during the heating stage, both PLSNCs show an apparent dual endothermal peak. It is well known that a crystalline phase-separated system commonly exhibits a dual melting point, which is caused by the different thermal stabilities of the resulting crystal phases. Therefore, our result suggests that there are two crystal populations present in both PLSNCs, corresponding to the α and γ crystals of nylon 6, which are qualitatively consistent with data from WAXS. As shown in the dual endotherm, the higher temperature peak at 221°C represents the melting point of α crystals of nylon 6, whereas the additional peak or shoulder at a lower temperature (ca. 210°C) results from imperfect, polymorphic γ crystals of nylon 6. The peak of the endotherm for the γ form in the HMW-NC is more pronounced than that in the LMW-NC. This indicates that the fraction of γ-form crystals increases with the molecular weight of the nylon 6 matrix, as measured by WAXS analysis (the peak areas are 26,130 for the HMW-NC and 25,700 for the LMW-NC). This occurrence seems to be explained by different degrees of phase interactions in the systems, which can markedly affect the crystal nucleation phenomena during the processing. It is likely that because of a higher weight-average molecular weight of nylon 6, the HMW-NC shows a larger phase dispersion and higher interfacial adhesion between the components than the LMW-NC, as supported by the morphological analysis of the PLSNCs, which is described later. The nonisothermal crystallization behaviors of both PLSNCs observed from DSC cooling scans at a rate of 10°C/min are very similar, exhibiting a single, sharp exothermal peak. However, the LMW-NC reveals a slightly higher crystallization temperature than the HMW-NC (185.8 and 181.8°C, respectively). This increase in the peak temperature indicates that the LMW-NC can be earlier crystallized upon cooling from the melt than the HMW-NC.

On the basis of the DSC results, we can make the following conclusion: the presence of large, anisotropic silicate monolayers plays an important role in the crystallization of the matrix. There is sufficient mobility for the two populations to segregate, yielding distinct crystalline populations. For a given LS content, the crystallization temperature of the nylon 6 matrix in PLSNCs decreases with the molecular weight of the matrix. At the same time, the LS induces strong heterophase nucleation of the γ crystals.

Morphology

To confirm the results of the dispersion of LSs in the nylon 6 matrix from WAXS, we performed a TEM investigation. Figure 4(a,b) shows typical morphologies of the HMW-NC and LMW-NC obtained from unstained ultrathin sections. In the TEM micrographs, the black lines with a thickness of about 1 nm represent the intersections of MMT LSs, whereas the gray part represents the nylon 6 matrix. From the TEM images, the degree of dispersion and the orientation of LSs in the nylon 6 matrices based on different molecular weights in the presence of the same amount of MMT (3.2 wt %) become clear.

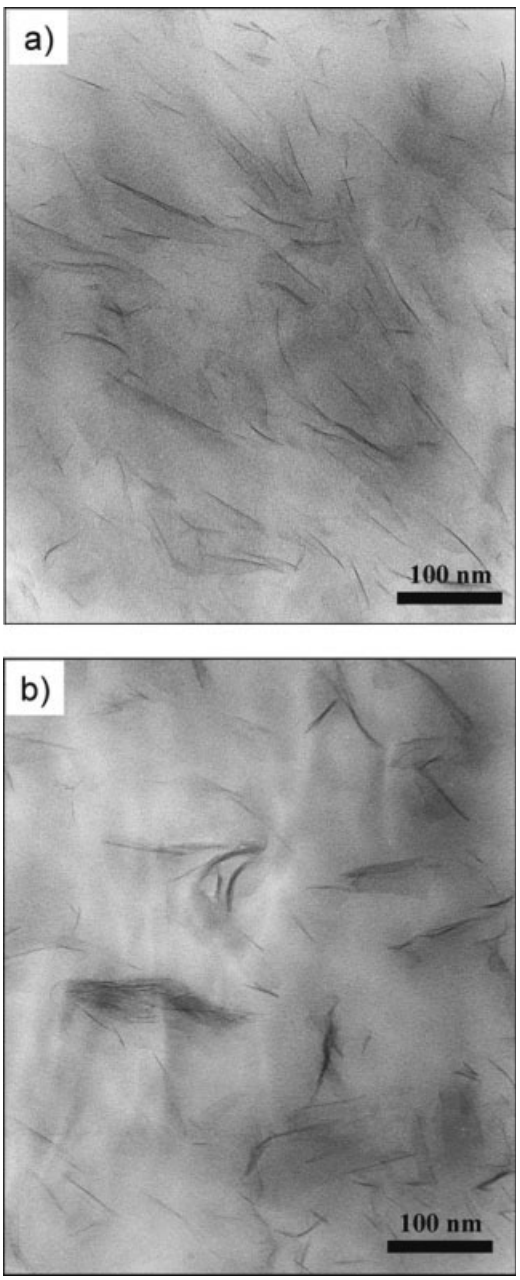

Figure 4 TEM micrographs of PLSNCs without a staining treatment: (a) the HMW-NC and (b) the LMW-NC.

As shown in Figure 4(a) for the HMW-NC, the individual LSs, along with two- and three-layer stacks,

are homogeneously well-dispersed (exfoliated) in the polymer matrix, in agreement with the WAXS results. In contrast, the LMW-NC shows a mixed nanomorphology [Fig. 4(b)] with coexisting intercalated tactoids and a partially exfoliated morphology, as also expected from WAXS measurements. It can be easily recognized in the TEM micrographs that the LSs in the HMW-NC are more likely to be oriented in the injection-molding direction analogously to conventional glass-fiber-reinforced polymer composites, whereas the LSs in the LMW-NC are relatively heterogeneously dispersed in the matrix, that is, showing no proper direction. This forced orientation is a result of the high shear rates during injection molding. It is reasonable to expect that the higher molecular weight systems, because of their higher melt viscosities, transfer more stress or energy to achieve the separation of LSs. Therefore, it can be assumed that high levels of shear stress in the HMW-NC aid in the breakup of clay particles and ultimately improve the degree of exfoliation, with a fair number of single layers as well as a few stacks of LSs. However, a low-molecular-weight matrix imparts low shear stresses to the agglomerates, which may skew the stacks of LSs rather than separate them, containing a relatively large percentage of nonexfoliated silicate particles in the form of intercalated tactoids, which are most difficult to align during injection molding. Thus, the LMW-NC is similar to conventional particle-filled polymer composites.

As mentioned previously, the LSs drastically affect the changes in the nylon 6 morphology. Because the nanoscopic arrangement of the crystal lamellae is comparable to the distribution of LSs, this is of crucial importance for understanding the structure–property relationship to characterize the phase morphology of PLSNCs. For this purpose, PLSNCs have been stained with OsO_4, and the resulting TEM micrograph is shown in Figure 5.

During the staining of nylon 6 with OsO_4, fine OsO_4 particles are preferentially precipitated at the most reactive, rigid–amorphous regions.[35,36] As a result, the lamellar structure of nylon 6 can be clearly recognized in the TEM micrographs, as shown as in Figure 5, which reveals lamellae by two parallel black lines.

In the HMW-NC, the nylon 6 lamellae are well defined and more oriented perpendicularly to the silicate interfaces in comparison with the LMW-NC. This result can be explained by the fact that a large extent of exfoliation in the HMW-NC leads to an increase in the surface area for polymer–LS interactions. At the crystallization temperature of the nylon 6 matrix, the surfaces of LSs act as heterogeneous nucleation sites. Once nucleation of the oriented lamellae occurs at the surfaces of LSs, the growing faces of the lamellae, that is, the hydrogen-bond planes, become parallel to the interfaces. As a result, the lamellae are oriented with chains lying tangential to the particle surface. In the LMW-NC, the LSs are not homogeneously dispersed in the matrix; therefore, the nylon 6 lamellae grow randomly, that is, revealing no proper orientation. Moreover, the individual LSs cannot clearly be seen in the TEM micrographs from OsO_4-stained sections. Generally, in melt-processed nanocomposites, polymer chains weakly interact with the LSs and are kinetically favorable for forming a γ phase in contact with the LSs. These γ crystallites are less stable and possess even more smaller, imperfect crystallinities because of the competition of the coverage with the $(HE)_2M_1R_1$ organic modifier at the surfaces of LSs and the presence of excess free volume associated with the packing constraints of intercalated chains. During the staining process with OsO_4, the staining agent will be preferentially incorporated into these defect zones. Furthermore, the lamellae in both systems (ca. 5 nm in the TEM micrographs) are comparably thicker than the LSs themselves. Therefore, if the lamellae are randomly dispersed around the LSs, the lamellae can fully cover the LSs, revealing a diffuse appearance around the LSs, in comparison with the unstained TEM micrographs in Figure 4. Moreover, we cannot distinguish between the α and γ phases in the TEM micrographs. This can be explained as follows: even though dense regions of the specimens, which scatter many electrons, might appear brighter than less dense regions, which scatter fewer electrons, the density difference between the α and γ phases is too small to produce a contrast change in TEM. Because of the extreme confinement of intercalated tactoids in the LMW-NC as well as

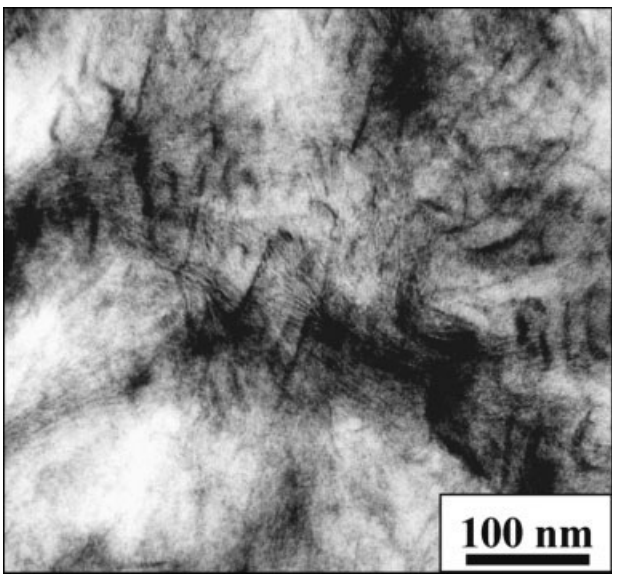

Figure 5 TEM micrograph of the HMW-NC with OsO_4-stained sections.

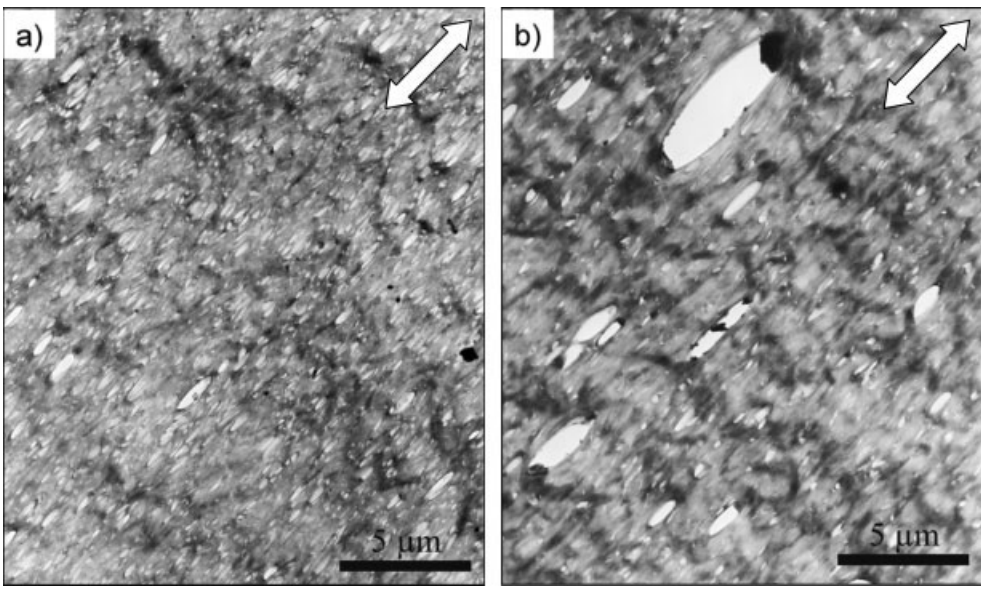

Figure 6 Characteristic deformation structures from *in situ* tensile experiments under HVEM: (a) the HMW-NC and (b) the LMW-NC.

two or three stacks of LSs in the HMW-NC, no evidence of crystallites has been observed in the interlayers. It can be concluded, therefore, that the polymers in the extremely confined interlayers seem to be in a completely amorphous state.

Deformation mechanism

To study the role of LSs in PLSNCs in deformation processes, we performed *in situ* deformation experiments with HVEM at an operating voltage of 1000 kV. Figure 6(a,b) shows HVEM micrographs of the deformation structures at a low magnification taken during *in situ* tensile tests for the HMW-NC and LMW-NC, respectively. The deformation structures reveal well-developed microvoid formation in the intercalated tactoids and around the exfoliated layers in the plastically deformed specimens.

On the basis of these observations, it can be concluded that the prominent deformation mechanism for nylon 6/LS nanocomposites is microvoid formation, which permits energy dissipation under an external load during plastic deformation processes. The remarkable differences exhibited in the TEM micrographs are the distribution and the size of the resulting microvoids. In the deformed HMW-NC [Fig. 6(a)], the microvoids, elongated in the tensile direction, are homogeneously distributed in the whole range of the deformed specimen and appear in the range of micrometers, whereas in the deformed LMW-NC, the microvoids appear randomly in the whole area of the deformed specimen; even the larger microvoids can be clearly seen in Figure 6(b). These differences in the deformation structures are clearly caused by their morphologies in both systems. It is likely that over a significant extent of exfoliation in the HMW-NC, the external subjected tensile stress is much more effectively transferred from the polymer matrix to the LSs because of the increased number of polymer–particle interactions. The microvoids are thus uniformly formed on the deformed specimen. In contrast, in the LMW-NC under an external load, the stress fields around the large tactoids are strongly overlapped by interactions with those of adjacent small stacks, which cause higher hydrostatic or triaxial stresses; therefore, void formation will easily take place around them.

To prove the exact role of individual LSs in the deformation mechanism in PLSNCs, it is important to find out where the microvoids will be initiated at the beginning of deformation processes. For this study, we selected the HMW-NC system because of the well-defined exfoliation of LSs in the polymer matrix. Figure 7 shows the deformation structures at the beginning of tensile tests on thin sections of the HMW-NC, which were taken from different areas in deformed specimens at a high magnification by TEM. Once the polymer matrix is activated to deform plastically, the voids preferentially initiate around the LSs. As can be clearly seen in Figure 7, we can find several microvoids and LSs with large curvatures located at the borders of the microvoids in the deformed specimens. Because the flexural rigidity of LSs is less than that of more isotropic spherical particles,[36] they are readily subjected to a large bending moment. As a result, the well-exfoliated individual LSs reveal highly folded structures in highly strained specimens (as shown at site I).

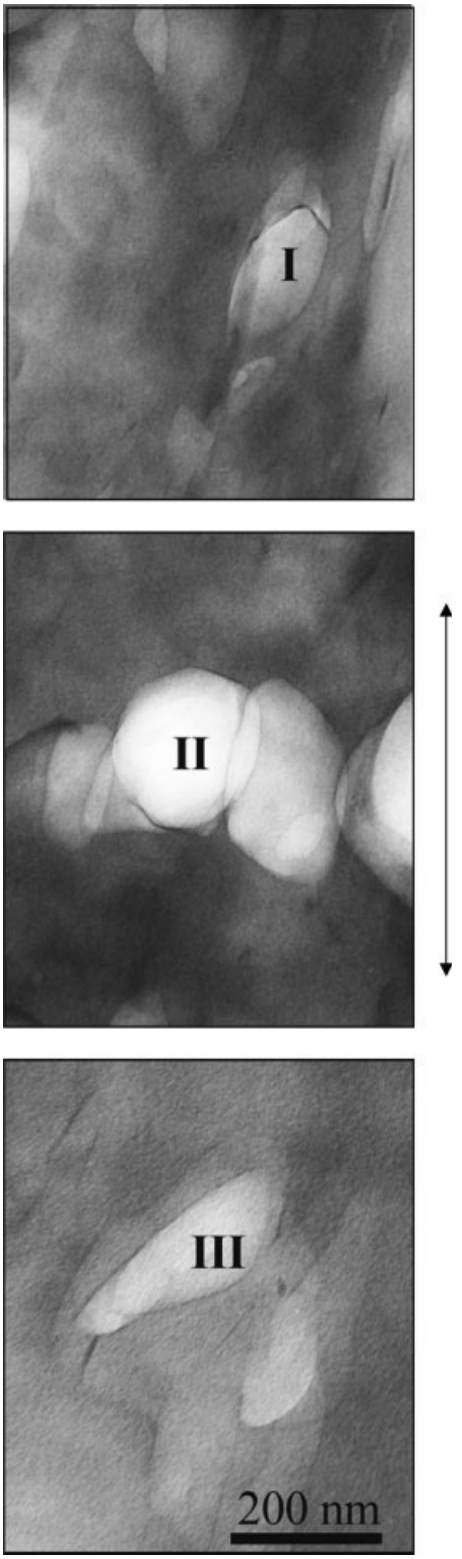

Figure 7 Deformation structures around individual LSs in the exfoliated HMW-NC.

As also discussed previously in this work,[33] the LSs are preferentially oriented in the injection-molding direction. This orientation of LSs plays a decisive role during deformation processes. When the LSs are closely stacked perpendicularly to the tensile direction, subsequently the microvoids initiate at middle areas between the stacked LSs. As the strain increases, the microvoids initiated inside stacked LSs grow in the tensile direction, as shown at site II in Figure 7. In the case of stacked LSs oriented at a certain angle to the applied stress, microvoids are generated between the stacked LSs and further grow acentrically during plastic deformation (as shown at site III).

DISCUSSION

In most conventional particle-filled polymer composites, the modulus increases linearly with the filler volume fraction, whereas for the PLSNCs, considerably lower LS contents sharply increase the modulus to a much larger extent. The dramatic enhancement of the Young's modulus for such extremely low LS contents cannot be simply ascribed only to the higher modulus of inorganic fillers.[37] The synergism in PLSNCs may originate from their final nanomorphology, which is associated with the high aspect ratio and the extremely large surface area exposed to the polymer. However, there is still a very moderate increase in the toughness observed. To obtain better insight into PLSNCs for improving and controlling the ultimate mechanical properties for wide-ranging applications (specifically the combination of stiffness and toughness), we now discuss the interrelationship between the morphology, mechanical deformation processes, and macroscopic mechanical properties.

On the basis of the results from DSC, WAXS, and TEM measurements, we suggest schematic representations for the formation of the morphology in nylon 6/clay nanocomposites, as illustrated in Figure 8(a,b), for the exfoliated and intercalated nanomorphologies, respectively. It has been shown in this work that the LSs induce strong heterophase nucleation of the crystallites of nylon 6, ultimately resulting in predominance of the γ form at the LS surfaces, whereas the α-phase crystallites are mostly well isolated from the LS surfaces.[30] This may result from conformational changes in the polymer chains, limiting the formation of H-bonded sheets, which leads to kinetically favored formation of the γ-crystal form at the LS surfaces. The amine end groups in nylon 6 are partially tethered to the LS surfaces by ionic bonding with the minus charge of the LSs, which are therefore easily incorporated into the interfacial ordering of the crystallite, leading to well-organized lamellae perpendicular to the LSs. This feature would be consistent with the well-known transcrystallization.[38] In contrast, the nonbonding chains of nylon 6 partially rearrange more readily into larger crystallite of the α form and do not grow in any

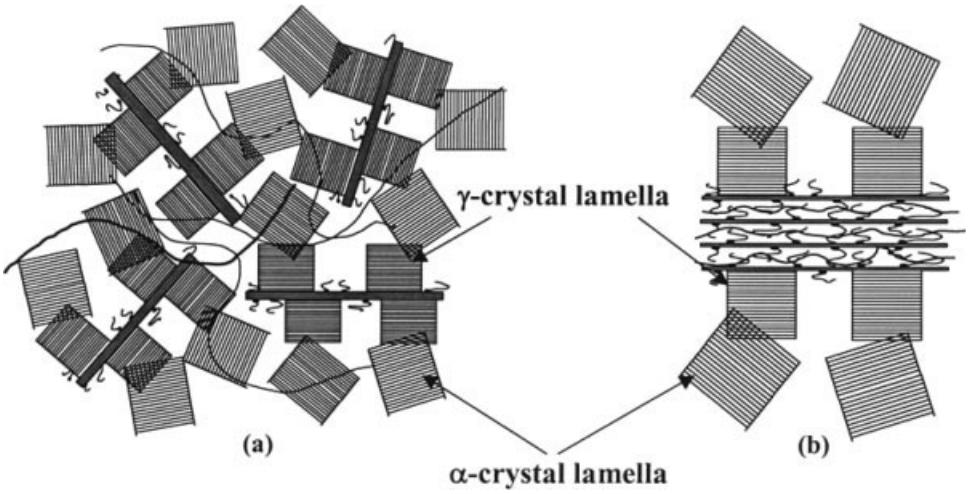

Figure 8 Schematic representation of the nanomorphology of (a) exfoliated and (b) intercalated PLSNCs.

preferential direction with respect to the LS surface. Thus, the average size of the α forms would be larger than that of the γ forms; moreover, they would have less perfect organization, allowing for more molecular mobility in the crystalline regions.

For semicrystalline polymers, the chains are confined in amorphous regions a few nanometers wide, whereas the intercalated polymer occupies a gap of less than 1 nm. Our WAXS results show that the *d*-spacing is 1.8 nm, indicating that nucleation sites could be confined within 0.8 nm (the 1-nm thickness of LS have been subtracted). On the basis of the geometrically extreme confinement in the interlayer, a large fraction of the intercalated polymer chains are in direct contact with the surface of the silicate. Topographically, the surfaces of the opposing silicate layers strongly restrict the motions of the polymer chains. In addition, the interactions of the polar polymer segments with the polar silicate surfaces and with the interlayer cations will bias the local motion of the polymer chain to certain energetically favorable orientations. Therefore, in the intercalated tactoids, the confined chain configuration is much more planar than the bulk polymer chains. In good agreement with the findings of others, the confinement of the polymer chains between the silicate layers effectively prohibits bulklike crystallization. One can assume that if the intercalated polymer could be crystallizable, the *d*-spacing would be expected to be more than several nanometers. However, no sign of crystal lamellae in the intercalated tactoids is evident in the TEM micrographs. This strongly suggests that the confined polymer could hardly be crystallized. As a result, the lamellae consisting of the γ form are located on the outer surfaces of the intercalated tactoids, not in the interlayer. Figure 8(a) illustrates the exfoliated nanomorphology. For the same concentration of LSs, the exfoliated nanomorphology can provide more surface area for interacting with polymer chains; as a result, the total fraction of crystallinity, particularly of the γ form, is higher than that in the intercalated nanomorphology. Furthermore, the polymer chains tethered to the LSs are less constrained than the intercalated tactoids, and this leads to higher mobility of the polymer chains. As a result, the more γ crystals there are in the exfoliated nanomorphology, the higher the ductility is without the sacrifice of the modulus, in comparison with that in the intercalated nanomorphology. The ductility of the polymers is primarily determined by the competition between the shear deformation resistance and the tensile strength of the samples. In general, nylon 6 exhibits a high tensile modulus because of strong hydrogen-bonding interactions. As mentioned previously, both systems studied in this work exhibit two crystalline modifications, namely, the α phase[39] and γ phase.[40] The α phase consists of fully extended, planar zigzag chains, in which the hydrogen bonds are formed between antiparallel chains. Therefore, it is the thermodynamically most stable crystalline form. The γ phase is less stable and is composed of twisted and pleated sheets of parallel chains joined by hydrogen bonds. Ito et al.[41] reported that the apparent ductility of nylon 6 crystals is higher for the γ form than for the α form. Thus, the deformation behavior of the two crystalline forms provides us with useful information on the mechanical properties of semicrystalline polymer nanocomposites.

Figure 9 presents a schematic illustration of mechanical deformation processes in intercalated tactoids. The γ forms generated as amine end groups in nylon 6 are more tightly bound by ionic interactions to the surface of the clay, which are expected to create an energetic barrier to the debonding (phase separation between the LSs and matrix) during plastic

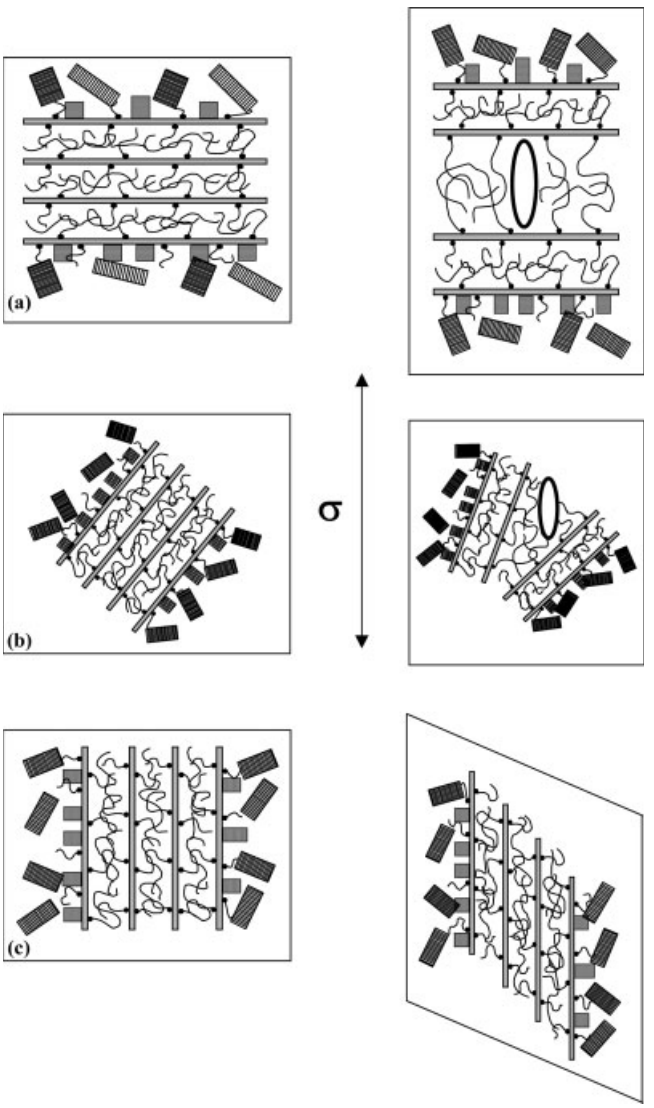

Figure 9 Schematic deformation processes in the intercalated nanomorphology system.

deformation. The presence of such stronger interactions restricts the mobility of the polymer chains of nylon 6. In addition, the mobility of the chains in the vicinity of LSs also could be greatly reduced by themselves. Under an external uniaxial load, such intercalated tactoids are readily subjected to high hydrostatic stresses, which can be released by the formation of microvoids. Because of the strong ionic bonds of nylon 6 to the LS surfaces, microvoids are caused not by debonding at the outer surfaces of the intercalated tactoids but by cavitation within the intercalated tactoids. As mentioned earlier, during the injection-molding process, for example in the LMW-NC, the LSs are not uniformly dispersed but are partially agglomerated with some extent of orientation to the injection direction in the matrix, appearing in the forms of intercalated tactoids. Deformation processes depend strongly on their orientation. Once the uniaxial load is applied at an intercalated tactoid, which is orientated perpendicularly to the applied load, deformation is initiated in the middle region of the intercalated tactoid; that is, splitting of the layer takes place in the middle region [Fig. 9(a)], the process of which has been called a splitting mode in a previous work. When an intercalated tactoid lies at a certain angle to the direction of the applied load, open bundles of the intercalated tactoids occur during deformation processes [Fig. 9(b)]; this is called an opening mode. As mentioned previously, because the confined polymer chains reveal much more planar configurations in the intercalated tactoids, when the intercalated tactoids are oriented parallel to the applied load, the slip of layers easily takes place during plastic deformation [Fig. 9(c)]; this is called a slipping mode.

In the exfoliated nanomorphology, the external subjected stresses are much more effectively transferred from the polymer matrix to the inorganic filler, and thus a higher increase in the Young's modulus is achieved. Furthermore, the uniformly well-developed formation of microvoids throughout deformed specimens and their subsequent growth should enhance matrix shear yielding, which is directly associated with energy dissipation during deformation; that is, it is reflected in the enhancement of the toughness of the system of exfoliated nanomorphology.

CONCLUSIONS

In this work, we prepared nylon 6/LS nanocomposites through melt blending to study their morphology and the role of LSs in local deformation processes. It has been shown that LSs induce strong heterophase nucleation of nylon 6 crystals, which results in the predominance of the γ form at the LS surfaces, whereas the α form is mostly isolated away from the LS surfaces. A TEM study has shown that a well-defined exfoliated nanomorphology can be observed in the nanocomposite with a high-molecular-weight matrix, whereas the nanocomposite with a low-molecular-weight matrix shows a mixed nanomorphology with coexisting intercalated tactoids and a partially exfoliated morphology. With the same content of the clay, the degree of exfoliation increases with the molecular weight of the polymer matrix. As for the density of the polymer–clay interaction sites, the exfoliated nanomorphology exhibits a large fraction of the γ form in comparison with the intercalated nanomorphology. These interactions significantly provide an energetic barrier to debonding (interfacial phase separation) during plastic deformation processes; the prominent deformation mechanism is microvoid formation, which is caused

by a cavitation process inside intercalated tactoids and/or at the vicinity of LSs in the matrix, by which applied energy is effectively dissipated during deformation processes. Additionally, the orientation of clay particles has an important role in the initiation of voids.

The authors thank Fornes and Paul at the Department of Chemical Engineering and Texas Materials Institute, University of Texas at Austin, for the kindly supplied samples, and Gösele at the Max-Plank Institute of Microstructure Physics in Halle/Saale for the use of a high-voltage electron microscope. They also give thanks to Krumova for carrying out the differential scanning calorimetry measurements.

References

1. Krishnamoorti, R.; Vaia, R. A. Polymer Nanocomposites: Synthesis, Characterization, and Modeling; American Chemical Society: Washington, DC, 2001.
2. Pinnavais, T. J.; Beall, G. W. Polymer–Clay Nanocomposites; Wiley: London, 2000.
3. Usuki, A.; Kojima, Y.; Kawasumi, M.; Okada, A.; Fukushima, Y.; Kamigaito, O. J Mater Res 1993, 8, 1179.
4. Giannelis, E. Adv Mater 1996, 8, 29.
5. Ogawa, M.; Kuroda, K. Bull Chem Soc Jpn 1997, 70, 2593.
6. Lan, T.; Pinnavaia, T. J. Chem Mater 1994, 6, 2216.
7. Cho, J. W.; Paul, D. R. Polymer 2001, 42, 1083.
8. Zilg, C.; Reichert, P.; Dietsche, F.; Engelhardt, E.; Mülhaupt, R. Kunststoffe 1998, 88, 1812.
9. Fornes, T. D.; Yoon, P. J.; Keskkular, H.; Paul, D. R. Polymer 2001, 42, 9929.
10. Usuki, A.; Kawasumi, M.; Kojima, Y.; Okada, A.; Kurauchi, T.; Kamigaito, O. J Mater Res 1993, 8, 1174.
11. Jordan, J. W. J Phys Colloid Chem 1949, 53, 294.
12. Lan, T.; Kaviratna, P. D.; Pinnavaia, T. J. Chem Mater 1998, 6, 1820.
13. Usuki, A.; Kato, M.; Okada, A.; Kurauch, T. J Polym Sci 1997, 63, 137.
14. Messersmith, P. B.; Giannelis, E. P. Chem Mater 1994, 6, 1719.
15. Carrado, K. A.; Xu, L. Q. Chem Mater 1998, 10, 1400.
16. Zeng, C.; Lee, L. J. Macromolecules 2001, 34, 4098.
17. Theng, B. K. G. Formation and Properties of Clay Polymer Complexes; Elsevier: New York, 1979.
18. Mehrotra, V.; Giannelis, E. P. Solid State Commun 1991, 77, 55.
19. Aranda, P.; Ruiz-Hitzky, E. Adv Mater 1990, 2, 545.
20. Parfitt, R. L.; Greenland, D. J. Clay Miner 1970, 8, 305.
21. Giannelis, E. Adv Mater 1996, 8, 29.
22. Vaia, R. A.; Ishii, H.; Giannelis, E. P. Chem Mater 1993, 5, 1694.
23. Vaia, R. A.; Jandt, K. D.; Kramer, E. J.; Giannelis, E. P. Macromolecules 1995, 28, 8080.
24. Vaia, R. A.; Giannelis, E. P. Macromolecules 1997, 30, 8000.
25. Ray, S. S.; Maiti, P.; Okamoto, M.; Yamada, K.; Ueda, K. Macromolecules 2002, 35, 3104.
26. Burnside, S. D.; Giannelis, E. P. Chem Mater 1995, 7, 1597.
27. Kato, M.; Usuki, A.; Okada, O. J Appl Polym Sci 1997, 66, 1781.
28. Laus, M.; Francesangeli, O.; Sandolini, F. J Mater Res 1997, 12, 3134.
29. Cho, J. W. D. R. Paul, Polymer 2001, 42, 1083.
30. Lincoln, D. M.; Vaia, R. A.; Wang, Z.-G.; Hsiao, B. S. Polymer 2001, 42, 1621.
31. Mathias, L. J.; Davis, R. D.; Jarrett, W. L. Macromolecules 1999, 32, 7958.
32. Vanderhart, D. L.; Asano, A.; Gilman, J. W. Chem Mater 2001, 42, 9929.
33. Kim, G.-M.; Lee, D. H.; Hoffmann, B.; Kressler, J.; Stöppelmann, G. Polymer 2001, 42, 1096.
34. Wu, T.-M.; Liao, C.-S. Macromol Chem Phys 2000, 201, 2820.
35. Suzuki, H.; Grebowicz, J.; Wunderlich, B. Macromol Chem 1985, 186, 1109.
36. Sawyer, L. C.; Grubb, D. T. Polymer Microscopy; Chapman & Hall: New York, 1987.
37. Shia, D.; Hui, C. Y.; Burnside, S. D.; Giannelis, E. P. Polym Compos 1998, 19, 608.
38. Stern, T.; Wachtel, E.; Marom, G. J Polym Sci Part B: Polym Phys 1997, 53, 2429.
39. Holmes, D. R.; Bunn, C. W.; Smith, D. J. J Polym Sci 1955, 17, 159.
40. Arimoto, H.; Ishibashi, M.; Hirai, M.; Chatani, Y. J Polym Sci Part A: Gen Pap 1965, 3, 317.
41. Ito, M.; Mizuochi, K.; Kanamoto, T. Polymer 1998, 39, 4593.